In Proceedings of "Int. High Level Radioactive Waste Management Conference"
April, 1992 Las Vegas, NV USA

X-RAY AND VISIBLE LIGHT TRANSMISSION AS TWO-DIMENSIONAL, FULL-FIELD MOISTURE-SENSING TECHNIQUES: A PRELIMINARY COMPARISON*

V. C. Tidwell, R. J. Glass
Geoscience Assessment and Validation Division, 6315
Sandia National Laboratories
Albuquerque, NM 87185
(505) 844-0945

ABSTRACT

Two independent high-resolution moisture-sensing techniques, x-ray absorption and light transmission, have been developed for use in two-dimensional, thin-slab experimental systems. The techniques yield full-field measurement capabilities with exceptional resolution of moisture content in time and space. These techniques represent powerful tools for the experimentalist to investigate processes governing unsaturated flow and transport through fractured and nonfractured porous media. Evaluation of these techniques has been accomplished by direct comparison of data obtained by means of the x-ray and light techniques as well as comparison with data collected by gravimetric and gamma-ray densitometry techniques. Results show excellent agreement between data collected by the four moisture-content measurement techniques.

I. INTRODUCTION

Experimentalists wishing to test hypotheses concerning flow and transport through unsaturated porous media have been limited by their ability to measure state variables in heterogeneous and/or transient systems. Recently, a number of tools for measuring moisture content in the laboratory have been developed beyond the standard gamma densitometer.[1] Examples include computed tomography (CT)[2,3] nuclear magnetic resonance (NMR),[4] electromagnetic tomography,[5] and microwave attenuation.[6] Each of these methods for measuring moisture content within laboratory test cells or in the field is limited in either spatial or temporal resolution, size of the sample, or in requiring very specialized and expensive equipment.

We have encountered similar limitations in our laboratory research program at Sandia National Laboratories. This program was established to support the Yucca Mountain Site Characterization Project through the development and validation of conceptual models for processes governing flow and transport through fractured and nonfractured unsaturated porous media.[7,8] To address our need for high-resolution, rapid moisture-content measurement in our laboratory research, we have explored thin but extensive experimental systems. In these two-dimensional slab systems, we have developed digital image-based full-field measurement techniques such as introduced by Glass[9] to obtain exceptional moisture-content resolution in both time and space.

In this paper, we discuss two full-field measurement techniques, one based on x-ray absorption and the other on light transmission. Moisture-content data as measured by each technique are compared, and both sets of data are compared with data collected by means of the more traditional techniques of gamma-ray densitometry and gravimetric analysis. The data have been collected from a series of experiments utilizing a thin-slab chamber filled with unconsolidated silica sands and subjected to a sequence of wetting and drying cycles.

We begin with a brief overview of x-ray and light transmission techniques and the theoretical basis for each. This is followed by a description of the experimental program aimed at the comparison of the techniques, then by the presentation of our results. Results show excellent agreement between data collected by the four moisture-content measurement techniques.

II. METHODS

In both the x-ray and light techniques, electromagnetic energy in the form of either x-rays or visible light is passed through the test media, and the moisture-content distribution integrated over the media's thickness is measured as variations in the transmitted x-ray or light intensity field. The difference between the techniques is in the frequency of the radiation used and in the physics governing the interaction that gives rise to variations in the transmitted

* This work was supported by the U.S. Department of Energy, Office of Civilian Radioactive Waste Management, Yucca Mountain Site Characterization Project Office, under contract DE-AC04-76DP00789

intensity field. In x-ray imaging, variations in the intensity field arise from the sensitivity of x-ray absorption to media density, which is directly related to moisture content (i.e., increase in moisture content yields a decrease in x-ray transmission). For the light technique, an increase in moisture content results in an increase in light transmission because of the closer matching of the index of refraction of the matrix and water relative to the matrix and air.

A critical factor governing the measurement of moisture content by means of x-ray transmission is the difficulty associated with achieving suitable image contrast. Contrast is defined here as the difference between the x-ray intensity field transmitted through the saturated test media to that transmitted through the dry test media. Difficulty arises because of the low density of water relative to that of the test media (silica). Theory dictates that image contrast may be improved by increasing media thickness and/or decreasing the intensity of the x-ray source;[10] however, the extent to which these parameters may be adjusted is limited by the sensitivity of the x-ray detecting device. Another alternative for increasing contrast, which is employed here, involves the doping of the water with a tracer to enhance x-ray absorption. The iodine ion, added in the form of potassium iodide (KI) was selected for two reasons:

- it is a conservative tracer, and
- it possesses favorable x-ray absorption properties for the range of x-ray source intensities used in this program.

One drawback to using the iodine tracer is the potential for limited interaction of the test solution with the porous media. A 10% solution (by weight) was used in these studies; however, solution strength may be decreased if an associated decrease in image contrast can be tolerated.

The critical requirement for the transmitted-light technique is that the porous media be translucent (i.e., silica sands, glass beads). This requirement also limits the thickness of the test media (on the order of a centimeter for most cases), and dictates that a high-intensity light source be used. In order to maintain a constant light-source-intensity level, light output from the source must be controlled through a feed-back circuit. Another impact is that the sensor, in our case a solid-state camera, must have a large dynamic range.

A. Measurement Techniques

For the light-transmission technique, imaging of the moisture-content field is accomplished by illuminating the back of the test media with a bank of high-output fluorescent lights while the variation in the transmitted-light intensity field is measured by means of a charged-coupled-device (CCD) camera focused on the front of the chamber. Camera output is digitized into an array of 512 by 512 points, with each point assigned a grey level between zero and 255 according to the light intensity. Such images can be recorded at a rate of up to 30 per second using our current video-imaging system.

Imaging of x-ray intensity fields is accomplished in much the same fashion as described above. Measurements are initiated by subjecting the test media to a collimated x-ray source. The transmitted x-ray intensity field is recorded on the back of the test media by means of x-ray-sensitive film. Once the film is developed it is digitized using the same lighting and camera system used in the light-transmission imaging.

B. Image Adjustments

Measurements made by both techniques are in terms of digitized grey-level data. These grey-level values are converted to water saturation through a two-step process. The first step adjusts the image to correct for variations in the light source and variations in film quality. In the second step, the adjusted grey-level values are converted to percent saturation by means of a functional relationship based on x-ray-absorption or light-refraction theory.

Image adjustment for the case of the light technique is required to correct for variations in the light-source strength. Adjustments to x-ray images also are required for this reason, as well as to correct for variations in image density resulting from temperature and time fluctuations in the film-development process and differences in film emulsion. Image adjustment is accomplished in the same manner for both the x-ray and light techniques. This procedure involves the incorporation of a variable-density wedge into each of the x-ray and light images. The wedge covers the complete range from dry to fully saturated and represents a constant by which adjustment can be accomplished. A curve is fit to the grey level/wedge density relationship associated with each image. An adjustment function then is obtained to map the curves for each of the images to that of an arbitrarily selected reference image. Grey-level values across the entire image then are corrected using the adjustment function.

C. Saturation Calculation: X-Ray Transmission

Once the x-ray images have been adjusted, it is then necessary to convert the data, which are in terms of grey level, to measures of moisture content. The percent saturation can be calculated by simply scaling the partially saturated image by the dry and fully saturated

images. The mapping of image grey-level values to saturation values is predicated on x-ray absorption theory.[11,12] For a polyenergetic x-ray source, the intensity of a transmitted x-ray beam, I, is proportional to the incident intensity, I_o, and the distance traversed by the beam. Thus:

$$\int_0^{kV} I(\beta)d\beta = \int_0^{kV} I_o(\beta)d\beta \left[\exp-\left(\rho_s x \int_0^{kV} \mu_s(\beta)\lambda(\beta)d\beta + \Theta x \int_0^{kV} \mu_w(\beta)\lambda(\beta)d\beta + \rho_c 2T \int_0^{kV} \mu_c(\beta)\lambda(\beta)d\beta\right)\right] \quad (1)$$

where kV is the maximum photon energy of the x-ray, β is the photon energy of the x-ray, λ is the x-ray wavelength, Θ is the moisture content, x is the test-media thickness, T is the thickness of the test-chamber walls, $\rho_{s,c}$ are the densities of the test media, and the chamber (glass in our case) respectively and $\mu_{s,w,c}$ sre the mass absorption coefficients for the test media, water, and container, respectively.

To represent I in terms of the light intensity transmitted through the x-ray image recorded on photographic film requires a relationship between the transmitted x-ray intensity and film exposure, E (a messure of the response of the film to an x-ray source of defined strength for a given period of time),

$$\int_0^{kV} I(\beta)d\beta = E/t \quad (2)$$

where t is the exposure time. The film exposure is related to transmitted light intensity, L, through the relationship:

$$E = E_o(L_o/L)^{1/\gamma} \quad (3)$$

where E_o is the saturation point of the exposure, γ is the slope of the film emulsion characteristic curve, and L_o is the intensity of the light incident on the x-ray film. Combining Equations 2, and 3 and substituting into Equation 1 yields:

$$\ln[E_o(L_o/L)^{1/\gamma}] - \ln[t \int_0^{kV} I_o(\beta)d\beta] = -F \quad (4)$$

where F represents the exponential term in Equation 1. We are able to scale grey level, L, to percent saturation, S, at each point in the image by the following relationship:

$$S = \frac{\ln(L) - \ln(L_d)}{\ln(L_s) - \ln(L_d)} \quad (5)$$

where L_d and L_s are the grey-levels for dry and saturated conditions, respectively.

D. Saturation Calculation: Light Transmission

Light transmission was first used by Hoa[13] to construct a sensor and quantitatively measure the moisture content point by point within a thin slab chamber filled with sand. His theoretical development may be applied directly within our context, as described below.

Light that passes through the porous media encounters sand, air, and water. Through each of these phases, light is absorbed exponentially as discussed above for x-rays. In addition, as light passes a diopter formed by a phase change (air-water, sand-air, sand-water) it is scattered and refracted, the transmitted intensity of the passing light being a function of the refractive indices of the two phases and the angle of incidence (microscale geometry). Assuming normal incidence, the ratio of emergent to incident light, referred to as the light transmission factor, τ, is given by Fresnel's law:

$$\tau = 4n/(n+1)^2 \quad (6)$$

where n is the ratio of refractive indices of the two phases. With the refrsctive indices of sand, water, and air (1.6, 1.33, 1.0, respectively), τ_{sw} for the sand-water diopter and τ_{sa} for the sand-air diopter are calculated to be 0.991 and 0.946, respectively. Thus if sand-water diopters replace sand-air diopters, emergent light intensity will increase.

If we assume that each individual pore is either full or empty of water, then the intensity of light transmitted across the system, I, is given by

$$I = A \exp[-(K_s - K_a)d_w] (\tau_{sw}/\tau_{sa})^{2p} \quad (7)$$

where A is the emergent light intensity for the dry sample, K_s and K_a are the light-absorption moduli of water and air, respectively, d_w is the sum thickness of water-filled pores and p is the number of pores filled with water. Since the difference between K_s and K_a is very small, we can approximate Equation 7 with

$$I = A (\tau_{sw}/\tau_{sa})^{2p} \quad (8)$$

Application of Equation 8 to calculate moisture content or saturation requires two additional steps. First, inhomogeneities in the lighting (mostly edge effects) and recording systems (sensor field) that do not result from moisture content must be removed. This is accomplished through the standard normalization procedure defining the normalized light intensity I_n, at a point

$$I_n = (I-I_d)/(I_s-I_d) \quad (9)$$

where I_d and I_s are the emergent light intensities for the dry and saturated conditions,

respectively. Second, a relationship between the number of pores filled with water, p, and the moisture content or saturation must be found. Hoa[13] argued that the relationship between p and the moisture content is unknown and so developed an independent empirical calibration curve between emergent intensity and saturation. In principle, however, the relation between p and the moisture content can be calculated from the moisture characteristic curve and capillary tube theory. Here, as a first step in seeking a simple functional mapping with physical significance, we make the assumption that

$$p = Sk \tag{10}$$

where S is the saturation and k is the average number of pores across the sample. Substitution of Equations 8 and 10 into Equation 9 and solving for S yields

$$S = \frac{\ln\left[I_n \left[(\tau_{sw}/\tau_{ss})^{2k} - 1 \right] + 1 \right]}{2k \ln[\tau_{sw}/\tau_{ss}]} \tag{11}$$

In principle, the average number of pores across the sample may be calculated from geometric arguments for regular or random packings. Another approach, used here, is to choose k to match the simplest, most readily available data for a given experiment. We define k by calculating the volumetric moisture content for the chamber using a suite of k values and then selecting the one that gives the best fit with the volumetric moisture content measured by gravimetric means. This second approach in combination with the simple approximation given in Equation 10 yields exceptionally good results.

III. METHOD COMPARISON EXPERIMENTS

The x-ray and light-transmission techniques have been compared to each other and to gravimetric and gamma techniques through a series of experiments conducted in a thin sleb chamber (25 cm wide by 60 cm tall by 1 cm thick) (Figure 1). Using the method of Glass et al.,[14] the chamber was filled homogeneously with silica sand. Three silica sands were used, 0.42-0.30

Figure 1. Light box, sand chamber, plumbing, and video-imaging equipment. The light box consists of a bank of high-output fluorescent tubes that are used to illuminate the back of the test media. The sand chamber, located directly in front of the light box, is fabricated from two 1.27-cm thick glass plates spaced 1.0 cm apart and attached to a screened baffle for introducing water into the bottom of the chamber. The plumbing on the right-hand side of the chamber is used to control the hydraulic boundary conditions as well as to monitor the mass of water moving into and out of the chamber. The transmitted light intensity field is captured by a CCD camera (not shown) whose signal is digitized and displayed on a computer terminal.

mm, 0.59-0.21 mm, and 0.84-0.149 mm, each differing only in their distributions about a common mean grain size. Each sand was subjected to three wetting and two drainage sequences using a 10% (by weight) KI solution. Each sequence was initiated with a change in boundary condition.

Fill 1: Starting in the initially dry condition, the chamber was filled from the bottom to saturation with 0 pressure haad at the top and 60 cm at the bottom.

Drain 1: The pressure head at the bottom of the chamber was decreased to 0 cm and the chamber drained slowly to equilibrium.

Fill 2: The pressure head at the bottom of the chamber was increased to 20 cm and the chamber filled slowly to equilibrium.

Fill 3: The pressure head at the bottom of the chamber was increased to 60 cm and the chamber filled slowly to equilibrium.

Drain 2: The pressure head at the bottom of the chamber was decreased to 30 cm and the chamber drained slowly to equilibrium.

Transmitted-light images were collected to follow the transient moisture changes within the chamber while the mass of water added to and drained from the chamber was monitored with time. Before Fill 1 (dry image) and after the chamber had reached equilibrium (at least 12 hours) following Fill 1, Drain 1, Fill 2, and Drain 2, the chamber was moved to the x-ray facility and then to the gamma facility to image the steady moisture content fields. Because of the time required to image the chamber using the gamma (approximately four hours), gamma data were collected for only the 0.42-0.30 mm sand.

X-ray imaging was conducted at the Non-Destructive Testing Laboratory at Sandia National Laboratories (Figure 2). Images were acquired with a Phillips, Model 420, industrial x-ray. The x-ray source strength used for imaging corresponds to a tube potential of 60 kV and tube current of 15 mA. The associated exposure time was 10.25 minutes. (primarily a function of the thick glass used in the sand chamber); the source-to-film distance was maintained at 2.5 m.

Gamma densitometry measurements were made with a 0.5 curie Cesium-137 source and measured by means of a collimated NaI scintillation detector. Critical measurement parameters include a 0.31 cm detector aperture, and a 30 second count time. Measurements were made at 1.0 cm spacings along vertical transects moving from

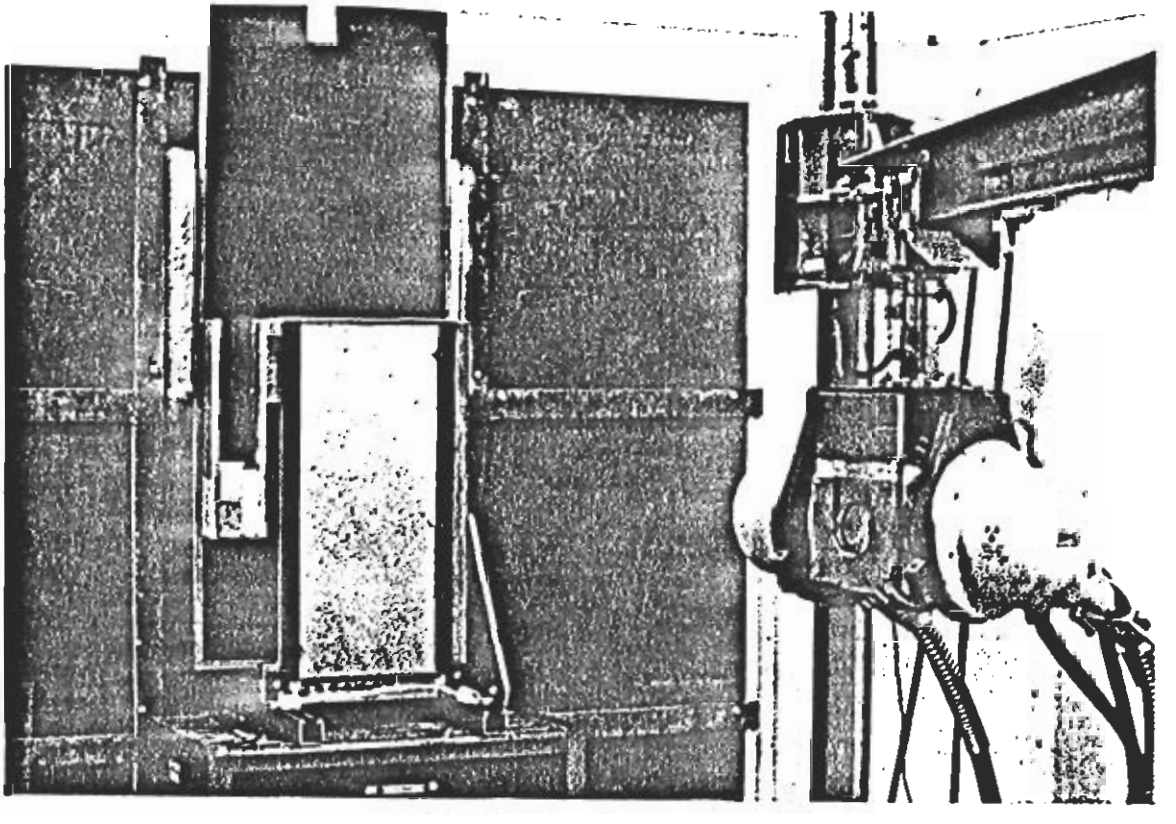

Figure 2. X-ray facility. X-ray images are acquired by subjecting the sand chamber to a collimated x-ray source. The transmitted x-ray intensity field is recorded on the back of the test media by means of x-ray sensitive film. Once the film is developed it is digitized using the same lighting and camera system as used in light-transmission imaging.

bottom to top of the sand chamber (total of 60 measurements). A total of five transects were made near the middle of the chamber, each spaced 1.0 cm apart. Automation of data acquisition and positioning of the gamma detector and source is accomplished through the use of computer hardware and software.

IV. RESULTS AND DISCUSSION

The accuracy of x-ray and light transmission as moisture-sensing techniques is evaluated by direct comparison with those techniques considered to be the standard in the soil sciences for laboratory measurement of moisture content in porous media (i.e., gamma densitometry and gravimetric analysis). Comparison is performed on the Drain 1, Fill 2, and Drain 2 images for each of the three sands tested (Figure 3). Three different types of comparison have been employed:

1) total volume of water in chamber,
2) average saturation profile with chamber height, and
3) direct point-by-point comparison of saturation fields measured by the x-ray and light techniques,

which represent a progression from the lowest to highest degree of moisture-sensing resolution.

Our first comparison is on the basis of the total volume of water within the chamber, as measured by x-ray, light, gamma, and gravimetric (based on independent mass-balance calculations) techniques. In Table 1, data concerning the total volume of water in the chamber are tabulated for all three experiments. A high degree of agreement is realized between the moisture data collected by the four independent methods. Average differences between the x-ray, light, and gamma total chamber moisture estimates

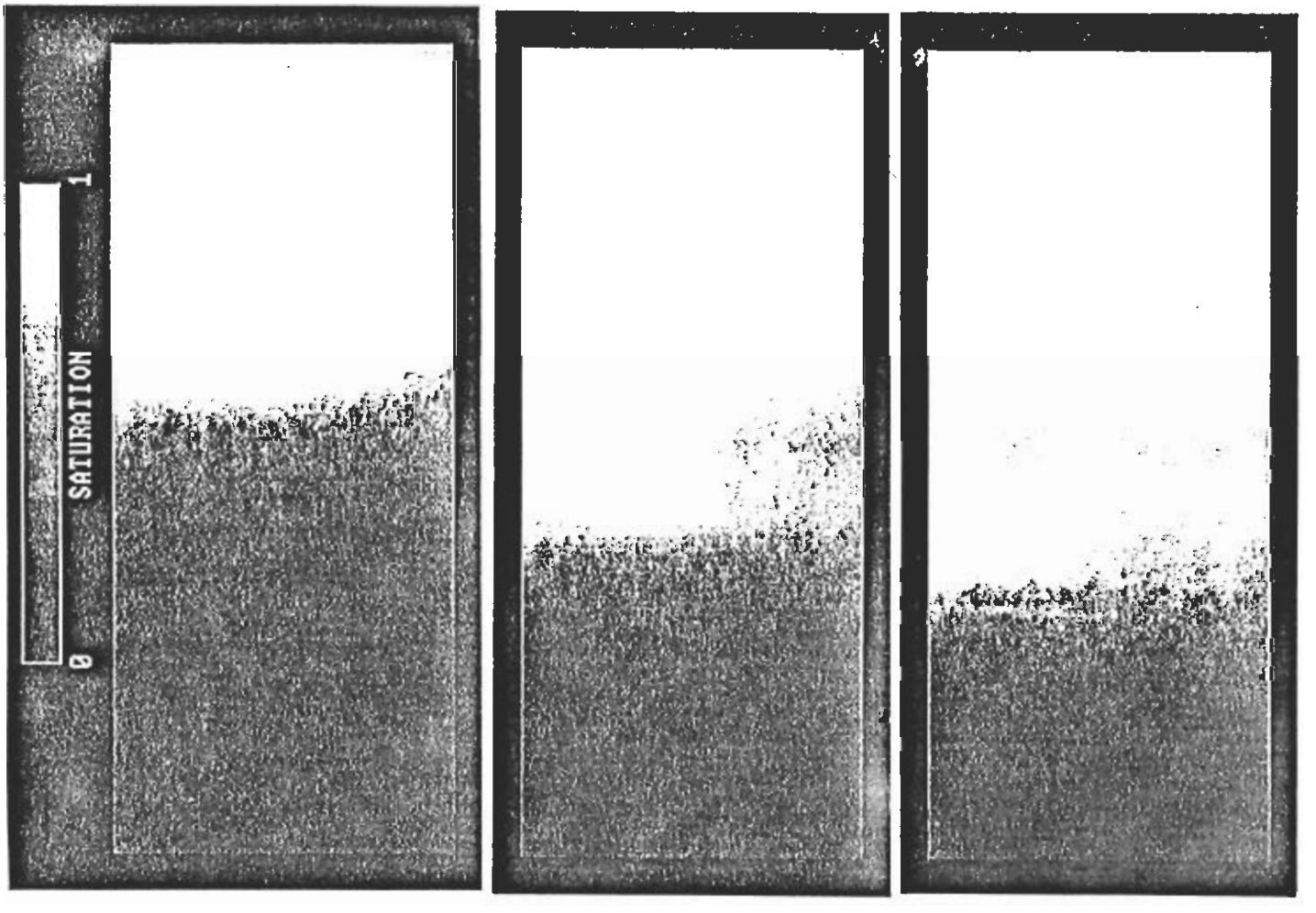

a. b. c.

Figure 3. Images representative of those used in comparison studies. This set of images is representative of the moisture saturation fields measured in each of the three experiments using the x-ray and light-transmission techniques: a) is representative of the Drain 1 series, b) of the Fill 2 series, and c) of the Drain 2 series.

Table 1. Total volume of water in chamber as measured by the x-ray, light, gamma, and gravimetric techniques (reported in ml).

Sand	Sequence	Gravimetric	X-ray	Light	Gamma
				k=19	
0.42-0.30 mm	Drain 1	325.7	328.7	329.6	327.0
porosity 0.3916	Fill 2	392.9*	413.0	412.9	396.3
theta 0.3818+	Drain 2	389.2*	406.6	405.4	388.7
				k=21	
0.59-0.21 mm	Drain 1	306.3	308.1	309.3	-
porosity 0.3817	Fill 2	420.1	426.6	426.3	-
theta 0.3625+	Drain 2	403.8	407.6	405.7	-
				k=33	
0.84-0.149mm	Drain 1	352.0	347.6	347.6	-
porosity 0.3688	Fill 2	407.9	407.9	410.1	-
theta 0.3482+	Drain 2	432.6	438.4	436.4	-

* Error in mass balance due to storage change during water injection after Drain 1

\+ Saturated moisture content

and that actually measured (gravimetric) are on the order of 5 ml. It should be noted that difficulties were encountered with the collection of the gravimetric data, especially in the case of the 0.42-0.30 mm sand, due to air entrapment within the bottom supply manifold that occurred when filling the chamber (may account for discrepancies on the order of 5-10 ml). In fact, the entrapment problem was manifest dramatically at the onset of the Fill 3 sequence for the 0.42-0.30 mm sand when formerly entrapped air escaped and fingered through the saturated region of the chamber.

Our second comparison is in terms of average saturation versus chamber height. Each point represents an arithmetic average for all points at that height in the chamber (Figures 4-6). The x-ray and light data represent an average of 235 points per height whereas the gamma data represent an average of 5 points. In addition, the x-ray and light data are taken at a height resolution of 8.4 data points per centimeter while the gamma data represents a 0.31-cm average at each centimeter of height. We note again that the gamma data were collected only for the 0.42-0.30 mm sand.

Agreement between the saturation profiles yielded by the three techniques is quite good. The average difference between curves is well below 10 grey levels (<5% saturation) with the greatest deviation being approximately 25 grey levels (10% saturation). Differences most commonly are encountered at the inflection points and in the low-moisture-content range. With respect to the inflection points, the gamma technique tends to underestimate relative to the x-ray and light techniques while the x-ray tends to initially underestimate and then overestimate saturation relative to the light technique. These discrepancies between the x-ray and light technique at the inflection points could be accounted for by temperature and orientation changes during transport to and from the x-ray and gamma facilities (discussed below).

To aid in the interpretation of the saturation profiles we also have plotted the saturation standard deviation as a function of chamber height for the 0.42-0.30 mm sand, which is considered to be representative of the other two experiments (Figure 7). For the sake of clarity we have omitted the light data since it follows very closely the trends in the x-ray data. Based on this comparison, we can see that the profiles generated by all three techniques fall within one standard deviation of each other. The standard deviation profiles also show very clearly that the gamma measurements are inherently more variable than those for the x-ray and light techniques (note the uncharacteristically higher variability in the saturated range of the Drain 2 x-ray data resulting from the escape of air entrapped in the supply manifold). Finally, it is worth noting the increase in variance in the moisture field outside the saturated region. This variance is not solely an artifact of the measurement technique but more of an indication of the variability in the saturation field itself. Because the light and x-ray techniques are applied at a spatial resolution of approximately three times the mean grain size, we actually are capturing near pore scale variation at a scale near to the pore size.

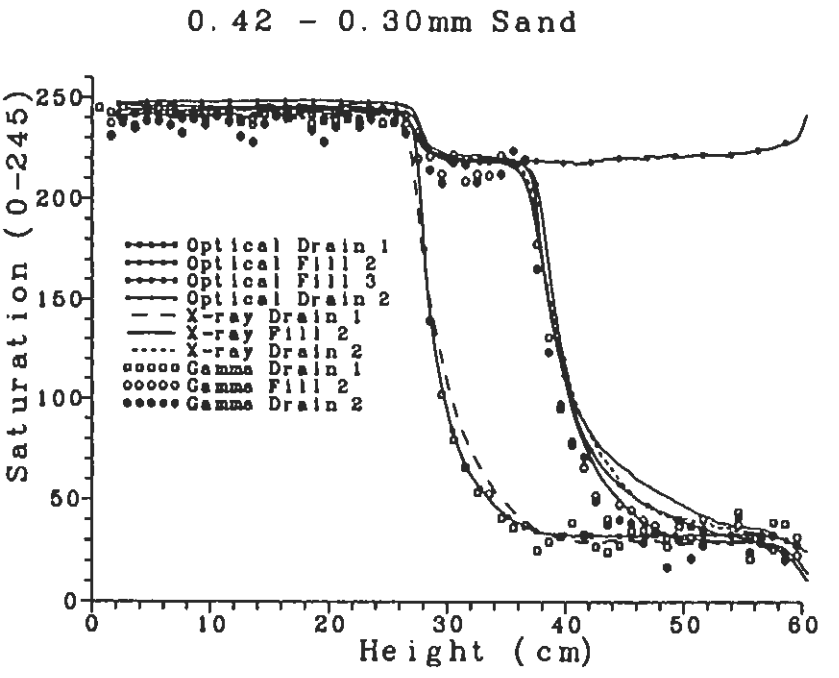

Figure 4. Saturation profile for the 0.42-0.30 mm sand. Saturation as a function of chamber height as measured by the x-ray, light, and gamma techniques. Saturation is defined in terms of grey level with zero representing an initially dry condition and 245 representing a saturated condition. Each point represents the arithmetic average for a single chamber height (average of 235 points per height for the x-ray and light data; average of 5 points for the gamma data).

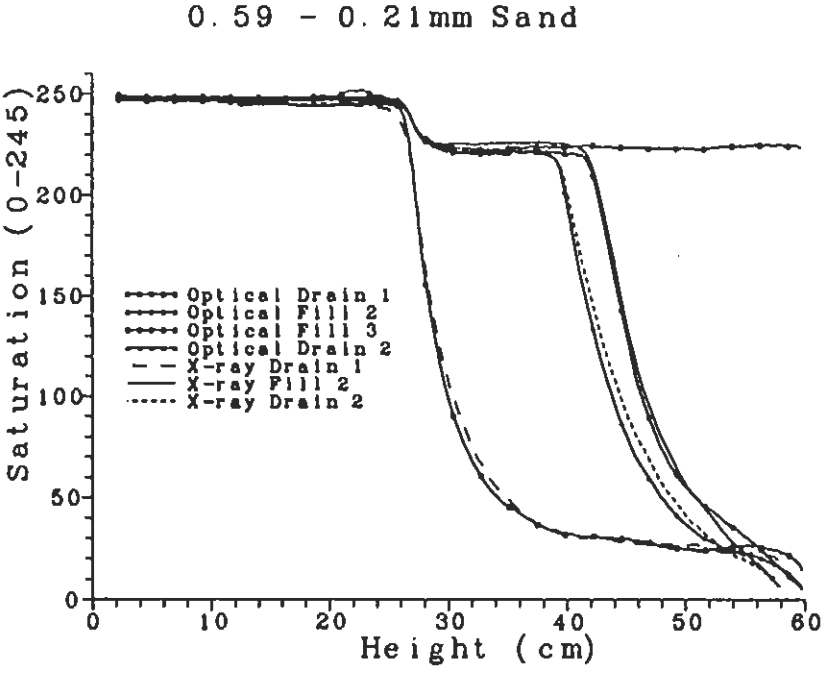

Figure 5. Saturation profile for the 0.59-0.21 mm sand. Saturation as a function of chamber height as measured by the x-ray and light techniques. Saturation is defined in terms of grey level with zero representing an initially dry condition and 245 representing a saturated condition. Each point represents the arithmetic average for a single chamber height (average of 235 points per height).

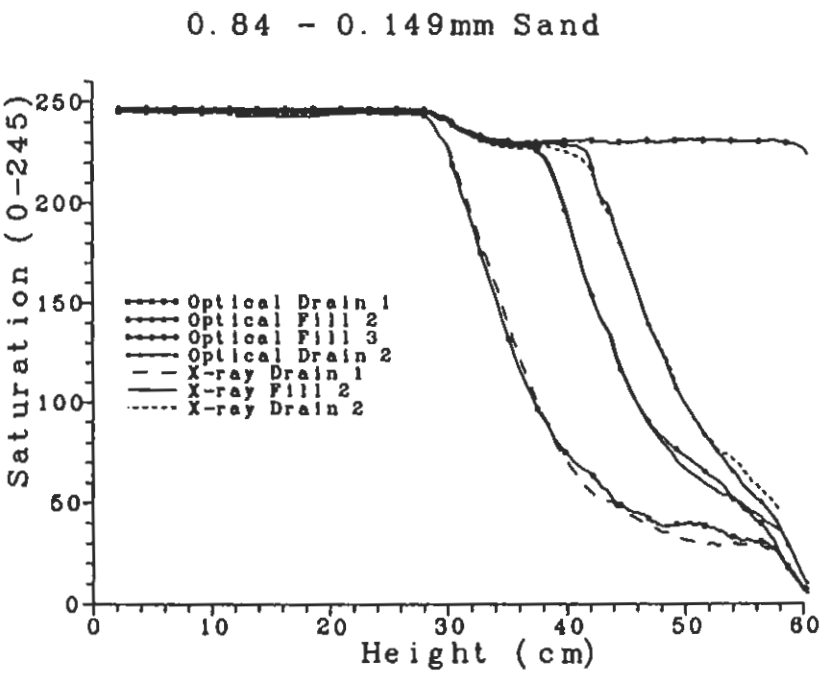

Figure 6. Saturation profile for the 0.84-0.149 mm sand. Saturation as a function of chamber height as measured by the x-ray and light techniques. Saturation is defined in terms of grey level with zero representing an initially dry condition and 245 representing a saturated condition. Each point represents the arithmetic average for a single chamber height (average of 235 points per

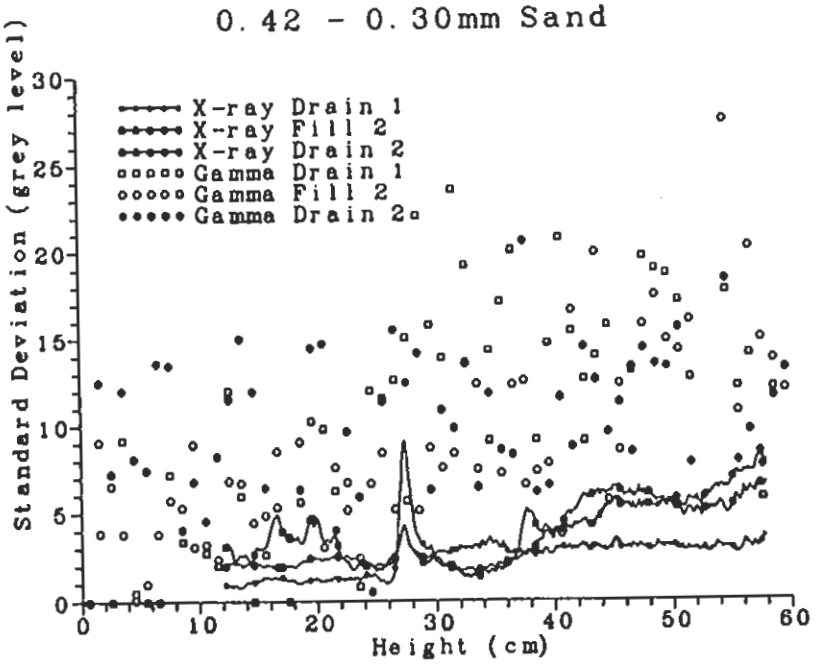

Figure 7. Saturation standard deviation profile as a function of chamber height as measured by the x-ray and gamma techniques. Shown here are the profiles for the 0.42-0.30 mm sand which are representative of the profiles for the other two experiments.

Our third comparison makes full use of the exceptional spatial resolution of the x-ray and light-transmission techniques. Here we compare the x-ray and light-transmission saturation fields point by point throughout the entire domain (265 by 384 points). Absolute-difference images are created that allow the visualization of discrepancies between the saturation fields measured by each technique. Two absolute difference fields, Fill 2 for the 0.42-0.30 mm sand, and Drain 2 for the 0.59-0.21 mm sand, are shown in Figure 8. These fields were selected because they represent the best and worst agreements between the two techniques within the nine saturation fields analyzed. The bright areas represent differences on the order of 20 grey levels (<10% saturation) which grades to black representing a zero absolute difference. Analysis of the absolute difference fields corroborate the conclusions drawn from the comparison of average-saturation and standard-deviation profiles. The isolated bright spots in the error fields result from metallic impurities in the sands that corroded over time (because of the KI solution) influencing light, but not x-ray, transmission.

One of the purposes for using three different sands (with broadening grain size distributions) was to evaluate the effect of pore-size distribution on the moisture-sensing capabilities of the x-ray and light techniques. In reference to our assumption in Equation 10 that allows a simple, one parameter, physically based relation between saturation and emitted light intensity, one would expect our prediction for at least the light technique to become less accurate as the grain-size distribution (and thus the pore-size distribution) widens. As indicated by Figures 4-6, this is not the case suggesting that Equation 11 is quite robust. In these figures, the moisture characteristics are shown to be sensitive to variations in the grain size distribution. In fact, as the grain-size distribution widens, a strong trend toward increased hysteresis and increased moisture dispersion about the transition points is evident. However, the relative difference between the x-ray and light transmission data remains consistent.

There are two catagories of error that were found to impact the experiments reported here:

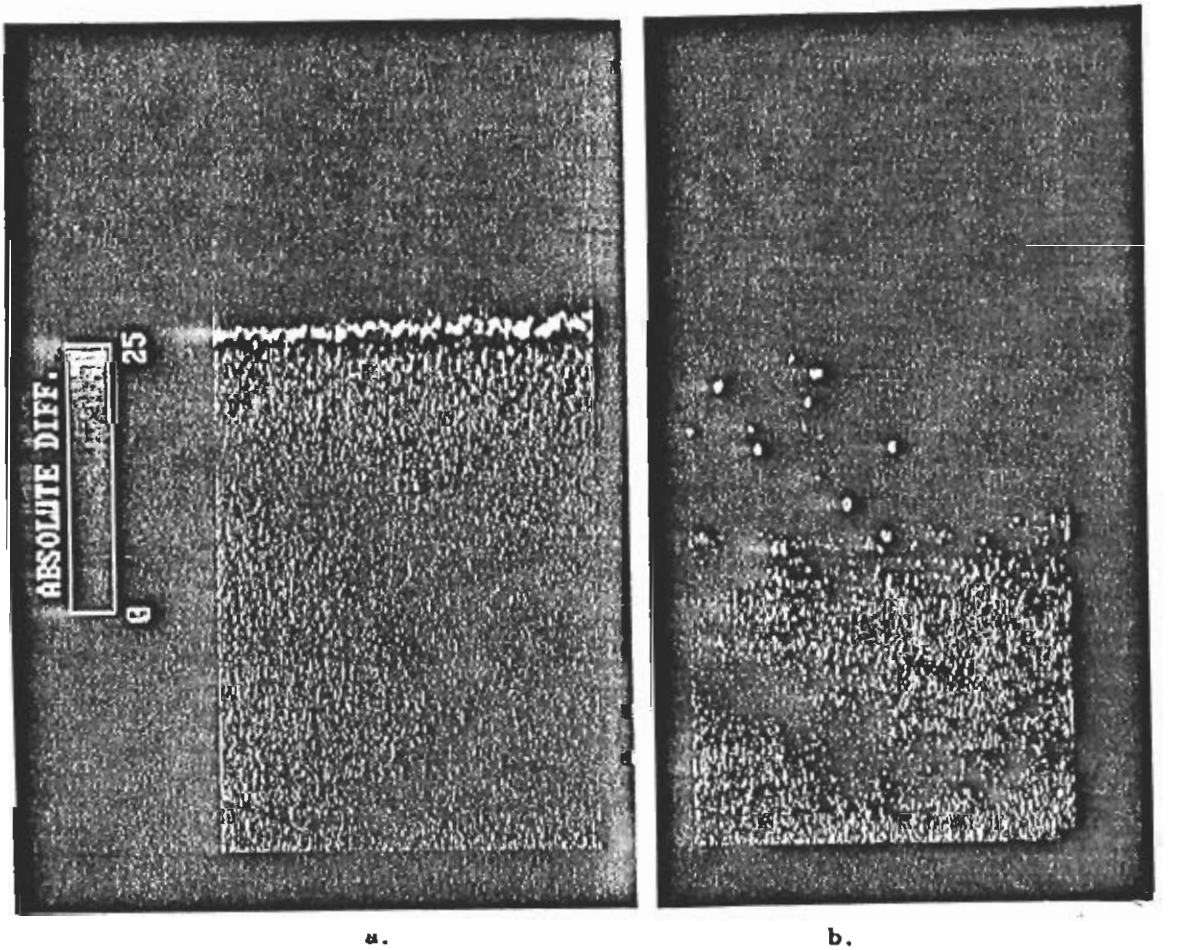

a. b.

Figure 8. Direct comparison of the full saturation fields as measured by the x-ray and light techniques. Two absolute difference fields, a) Fill 2 for the 0.42-0.30 mm sand, and b) Drain 2 for the 0.59-0.21 mm sand, are shown.

those resulting from our comparison program and those intrinsic to the full-field measurement technique. Our comparison program required us to move the experiment between three facilities and to use a concentrated KI solution which was not necessary for the light transmission technique. During experiment transport, temperature variations of up to 20 degrees C were experienced which caused expansion and contraction in the trapped air within the bottom supply manifold. In addition to chamber tipping while negotiating stairways and doors, high winds also were experienced while we carried the experiment the 0.5 kilometer distance between facilities. The temperature and tipping problems were greatest during our first test with the 0.42-0.30 mm sand, for which we found the greatest discrepancy in the saturation fields at the inflection points (where expansion or tipping would have their greatest effects).

At each facility, the experiment also had to be aligned properly with respect to the radiation source and sensor. Perfect alignment was impossible, resulting in about a 1-2 mm misalignment each time the chamber was moved, which in turn could cause a normal discrepancy of from 1-2 grey levels, and up to 10 grey levels where moisture conditions are rapidly varying. Corrosion of metallic impurities by the KI solution are responsible for localized discrepancies on the order of 20 to 25 grey levels between the x-ray and light images (x-ray images being of a higher intensity).

There are three sources of error intrinsic to the full-field measurement techniques as currently implemented: video camera signal noise (2-3 grey levels), variation of light-field uniformity with time, and variation in spatial uniformity of x-ray film/processing. Video camera signal noise can account for discrepancies in the total volume of water in the chamber of about 1-2 ml in our experiments. It is worth noting that measurement of the total volume of water in the chamber by the light and x-ray techniques never deviated by more than 2.2 ml. Camera noise can, of course, be reduced with more sophisticated and expensive, cooled digital cameras. While our image-adjustment procedure accounts for variations in the average light output and x-ray film development process, temporal light field and x-ray film uniformity variability still exist. This process, however, is difficult to entirely remove.

V. CONCLUSIONS

Two powerful techniques for measuring transient moisture-content fields in thin, two-dimensional experimental systems composed of porous materials at high spatial and temporal resolution have been developed. These techniques have the exceptional quality that in the time it takes to measure a single point by one of the traditional techniques, an entire image consisting of more than 262,000 points can be acquired by the x-ray and light techniques. However, as with any measurement technique, there are some limitations of which one must be aware, such as the requirement to use a non-opaque medium for the light technique and the need for a more highly absorbing liquid than water for the x-ray technique.

These techniques have been developed to support systematic experimentation to understand processes governing flow and transport through fractured and nonfractured unsaturated porous media; specifically in support of the Yucca Mountain Site Characterization Project. A number of applications have been realized for these techniques. These include the imaging of moisture content fields in highly heterogeneous materials such as volcanic tuff or cross-bedded and micro-layered unconsolidated media (similar to bedded tuffs). These techniques also are capable of imaging moisture distributions in fractures oriented normal to the imaging plane. As a result, the technique will facilitate fracture-matrix interaction studies to be conducted in thin slabs of fractured tuff and in analogue materials composed of sintered glass beads.[9] Although not explored in these experiments, both techniques also are capable of measuring solute concentration fields and bulk density fields at a resolution comparable to that in moisture-content investigations.

ACKNOWLEDGMENTS

We would like to extend our appreciation to a number of people who were instrumental in this research. Lee Orear helped in the development of the optical system and numerous software tools; Craig Ginn was responsible for design and fabrication of much of our test equipment; Ragimera Amato helped in data collection and reduction; Deanna Sevier aided in the collection of our x-ray images; and Anthony Russo allowed us access to the gamma facility and gamma data-reduction programs. R. J. Glass also acknowledges support of EPA grant #R81-2919-01-0 and the help of J. Throop of Cornell University during his initial development of the light-transmission technique in 1988.

REFERENCES

1. W. H. GARDNER, "Water Content,"in Methods of Soil Analysis, Ed. A.L. Page, R.H. Miller, and D.R. Kenney, American Society of Agronomy, 493-541 (1982).

2. S. CRESTANA, S. MASCARENHAS, and R. S. POZZI-MUCELLI, "Static and Dynamic Three-Dimensional Studies of Water in Soil Using Computed Tomographic Scanning," Soil Science, 140, 326-332 (1985).

3. S. H. ANDERSON, C. J. GANTZER, J. M. BOONE, and R. J. TULLY, "Rapid Nondestructive Bulk Density and Soil-Water Content Determination by Computed Tomography," Soil Sci. Soc. Am. J., 52, 35-40 (1988).

4. G. A. MATZKANIN and R. F. PAETZOLD, "Measuring Soil Water Content Using Pulsed Nuclear Magnetic Resonance," ASAE Technical Paper No. 82-2619, Am. Soc. Agric. Engr., St. Joseph, MI (1982).

5. W. DAILY and A. RAMIREZ, "Evaluation of Electromagnetic Tomography to Map In Situ Water in Heated Welded Tuff," Water Resources Research, 25, 1083-1096 (1989).

6. V. R. LATORRE and H. D. GLENN, "Microwave Measurements of the Water Content of Bentonite," in Proceedings of the Second Annual International High Level Radioactive Waste Management Conference, Las Vegas, 1, 578-582 (1991).

7. R. J. GLASS, "Laboratory Research Program to Aid in Developing and Testing the Validity of Conceptual Models for Flow and Transport Through Unsaturated Porous Media," Proceedings of the Geoval-90 Symposium, May 14-20, 1990, Stockholm, Sweden (SNL paper SAND89-2359C) (1989).

8. R. J. GLASS and V. C. TIDWELL, "Research Program to Develop and Validate Conceptual Models for Flow and Transport Through Unsaturated, Fractured Rock," in Proceedings of the Second Annual International High Level Radioactive Waste Management Conference, Las Vegas, 2, 977-987, (SNL paper SAND90-2261) (1991).

9. R. J. GLASS, T.S. STEENHUIS, and J.-Y. PARLANGE, "Mechanism for Finger Persistence in Homogeneous, Unsaturated, Porous Media: Theory and Verification," Soil Sc., 148:60-70 (1989).

10. E. M. KRAVCHUK and E. A. STRASHKEVICH, "Sensitivity and Accuracy of the Roentgenoscopic Method of Determining Moisture Content in a Porous Body," (translated from Inzhenorno-Fizicheskii Zhurnal, 25) 859-863 (1973).

11. J. G. BROWN, X-rays and Their Applications, Plenum Press, New York (1966).

12. E. F. KAELBLE, Handbook of X-Rays, McGraw-Hill, New York (1967).

13. M. T. HOA, "A New Method Allowing the Measurement of Rapid Variations in Water Content in Sandy Porous Media. Water Resources Res. 17(1);41-48 (1981).

14. R. J. GLASS, T. S. STEENHUIS, and J-Y PARLANGE, "Wetting Front Instability II: Experimental Determination of Relationships Between System Parameters and Two Dimensional Unstable Flow Field Behavior in Initially Dry Porous Media," Water Resources Res., 25, 1195-1207 (1989).